Front. Earth Sci. 2019, 13(3): 588–595
https://doi.org/10.1007/s11707-018-0743-7

RESEARCH ARTICLE

Analysis of ship wake features and extraction of ship motion parameters from SAR images in the Yellow Sea

Kaiguo FAN[1,2], Huaguo ZHANG[2], Jianjun LIANG[3], Peng CHEN (✉)[2], Bojian XU[1], Ming ZHANG[4]

1 P.O. Box 5136, No. 22, Beiqing Road, Haidian District, Beijing 100094, China
2 State Key Laboratory of Satellite Ocean Environment Dynamics, Second Institute of Oceanography, Ministry of Natural Resources, Hangzhou 310012, China
3 Key Laboratory of Digital Earth Science, Institute of Remote Sensing and Digital Earth, Chinese Academy of Sciences, Beijing 100094, China
4 College of Information Science and Engineering, Linyi University, Linyi 276000, China

Abstract The identifying features of ship wakes in synthetic aperture radar (SAR) remote sensing images are of great importance for detecting ships and for extracting ship motion parameters. A statistical analysis was conducted on the identifying features of ship wakes in SAR images in the Yellow Sea. In this study, 1091 ship wake sub-images were selected from 327 SAR images in the Yellow Sea near Qingdao. Analysis of the identifying features of ship wakes in SAR images revealed that both turbulent wakes and Kelvin wakes account for the majority of ship wakes, with turbulent wakes occurring approximately four times as frequently as Kelvin wakes. Narrow-V wakes and internal wave wakes were comparatively rare, which is due to the peculiarities of the radar system parameters and marine environments required to observe these wakes. Additionally, we extracted ship motion parameters from four types of ship wakes in the SAR images. Specifically, internal wave wakes in SAR images in the Yellow Sea were also used to extract ship motion parameters. Validation of the extracted parameters indicated that the extraction of these parameters from ship wakes is a viable and accurate approach for the acquisition of ship motion parameters. These results provide a solid foundation for the commercialization of SAR-based technologies for detecting ships and extracting ship motion parameters.

Keywords synthetic aperture radar, remote sensing, ship wake, ship motion parameter

Received January 25, 2018; accepted November 5, 2018

E-mail: chenpeng@sio.org.cn

1 Introduction

Ship wakes are the wave patterns left on water surfaces by a moving ship. These patterns are an important reference for detecting ships and for extracting ship motion parameters via remote sensing technologies (Ouchi, 2013). In synthetic aperture radar (SAR) remote sensing images, ship wakes usually appear as straight lines that extend over several kilometers, for up to tens of kilometers, and also may last from several minutes up to several hours. Since it is easier to detect ship wakes than the ships themselves in low-resolution remote sensing images, ship wake features help to improve the accuracy of ship detection and reduce the occurrence of false detections (Tings and Velotto, 2018). Furthermore, the Doppler shift of a moving ship can be corrected using ship wakes (Jackson and Apel, 2004), which improves the accuracy of ship detection and positioning via remote sensing technologies.

The earliest studies on ship wake features in remote sensing images were performed in the 1970s (Vesecky and Stewart, 1982; Swanson, 1984). In 1978, scientists first observed ship wakes from Sea Satellite (SEASAT) SAR images, and these ship wakes appeared in SAR images as dark lines behind ships that could extend for up to 24 km. The United States (U.S.) Office of Naval Research (US-ONR) subsequently began to fund hydrodynamic studies on ship wakes. Many studies have since been performed on the mechanisms of SAR imaging at different frequencies and on the identifying SAR features of different ship wakes. The SAR imaging mechanisms of different ship wakes in the X-band and L-band were classified by Lyden et al. (1988) using data collected by the Joint Ocean Wave Investigation Project (JOWIP). On this basis, they

attributed narrow-V wakes and Kelvin wakes to ship-generated surface waves. Additionally, Lyden et al. (1988) analyzed the classification of ship wake patterns in SAR images and the SAR imaging mechanisms that generate these patterns. In 1987, a joint experimental study was conducted by the U.S. and United Kingdom (U.K.) on the SAR imaging of internal wave wakes (Skoelv et al., 1988). In Loch Linnhe in Scotland, Hogan et al. (1994) compared the K_a, K_u, X-, and C-band SAR images of ship-generated internal wave wakes with spar buoy data. Ouchi et al. (1997) studied the ship-generated internal wave wakes in the P-, L-, and C-bands SAR images. Hennings et al. (1999) studied the SAR imaging mechanisms of Kelvin wakes using the Wigley model and found that the imaging of Kelvin wakes is mainly attributable to tilt modulation; it is also dependent upon factors, such as radar polarization, radar incidence angle, and wind speed on the sea surface. Based on these results, the ship wakes of moving ships in SAR images can be classified into four general categories: 1) narrow-V wakes, 2) Kelvin waves, 3) turbulent wave wakes, and 4) internal wave wakes. Both narrow-V wakes and Kelvin waves are generally caused by ship-generated surface disturbances, and the both waves may be further classified as surface wave wakes.

Typically, narrow-V wakes contain short (centimeter-scale) waves, which may be observed by SAR via the Bragg scattering mechanism (Stapleton, 1997). An alternative (and controversial) explanation for the observation and generation of narrow-V waves is the mixing of both the short and divergent Kelvin waves with the unsteady surface waves that are generated by ship-induced turbulence (Munk, 1987; Zilman and Miloh, 1997). Kelvin wakes, which contain long (decimeter-scale) waves, form the typical Kelvin waves. Turbulent wakes are generally caused by horizontal vortices along the sides of ship hulls and a net rearward velocity at the stern. This suppresses surface waves along the ship track and weakens their radar backscatter, which causes the ship track to appear as a dark line in SAR images. In contrast, surface waves on the sides of a ship are enhanced by the aforementioned horizontal vortices and net rearward velocity, which increases the radar backscatter of these waves and makes them appear as bright tracks in SAR images (Lyden et al., 1988; Zilman et al., 2015). Synthetic aperture radar imaging of internal wave wakes is dependent upon the marine environment. When a pycnocline is present, internal waves may be generated by ship motions or vortices along the sides of the hull. The motion and propagation of internal waves causes changes in surface current fields, which in turn modulate the spatial distribution of small-scale surface waves. This subsequently alters the radar backscatter of the sea surface, thus enabling the imaging of internal waves by SAR (Lyden et al., 1988; Fan et al., 2015). However, it is not always possible to detect all of the aforementioned types of wakes in SAR images, as the image features of ship wakes are affected by the intrinsic properties of ships, the marine environment, and the parameters of the SAR system (Hennings et al., 1999).

Meanwhile, scientists around the world have also investigated the frequency of different types of ship wakes in SAR images. Melsheimer et al. (1999) statistically analyzed more than 400 ship wakes in SAR images and over 100 ship wakes in Satellite Pour l'Observation de la Terre ("Satellite for the Observation of Earth", SPOT) satellite images. They found that turbulent wakes are present in nearly all ship wakes, and typical, dark turbulent wakes, bright turbulent wakes, and a combination of dark and bright turbulent wakes were found in 1/2, 1/3, and 1/6 of all cases, respectively, while Kelvin wakes accounted for approximately 17% of the wakes.

Although there is large body of research on the future use of ship wakes in China and abroad, there is no precedent in China for statistically analyzing the identifying SAR features of ship wakes or for using SAR images of ship-generated internal wave wakes to extract ship motion parameters. This gap in the literature may be attributed to deviations in the spatial positioning of SAR images, an insufficient number of samples for statistical analysis, and a lack of synchronously acquired hydro meteorological data (Zilman et al., 2004; An et al., 2018). Consequently, statistical analysis of the identifying SAR features of ship wakes and the extraction of ship motion parameters from the SAR images of ship-generated internal wave wakes have yet to be performed in a systematic manner in the seas of China.

In this study, we generated a dataset of ship wake-containing SAR images. Using this dataset, statistical analyses were performed on the identifying SAR features of ship wakes in the Yellow Sea. Additionally, a systematic study was also conducted on the extraction and validation of ship motion parameters using a variety of SAR ship wake features, including the SAR images of ship-generated internal wave wakes based on a continuous series of multi-temporal SAR images of the Yellow Sea near Qingdao in combination with sea surface wind speed data, conductivity, temperature, and depth (CTD) data, and synchronous Automatic Identification System (AIS) data.

2 Statistical analysis of ship wake features in SAR images

In this study, we generated a dataset (shown in Table 1) of 327 ship wakes-containing SAR images and 1091 ship wake samples, which consisted of 176 Environmental Satellite (ENVISAT) advanced SAR (ASAR) images and 151 European Remote-Sensing Satellite 1 and 2 (ERS-1 and ERS-2) SAR images corresponding to the Yellow Sea near Qingdao. These images span the period from 1991 to 2007. In the 327 SAR images shown in Table 1, 193 are Image Mode Precision (IMP) products, 10 are Image Mode Medium resolution (IMM) products, 78 are Alternating

Table 1 Calculated ship wake probabilities

Operational mode	Product ID	No. of images	Pixel spacing	No. of narrow-V wakes	No. of Kelvin wakes	No. of turbulent wakes	No. of internal wave wakes
Image	IMP	193	12.5	6	166	482	7
Image	IMM	10	75	1	3	7	2
Alternating Polarization	APP	78	12.5	2	34	257	4
Wide Swath	WSM	46	75	-	5	115	-
Sum				9	208	861	13
Calculated probability				0.8%	19.1%	78.9%	1.2%

Polarization Precision Image (APP) products, and 46 are Wide Swath Mode Medium resolution (WSM) products. The IMP and APP SAR images have a pixel spacing of 12.5 m, while the AMM and WSM SAR images have a pixel spacing of 75 m.

Using this dataset, ship wake features were analyzed and statistical analyses were performed on narrow-V wakes, turbulent wakes, Kelvin wakes, and internal wave wakes based on the SAR imaging mechanisms of each type of ship wake. Between the 1091 ship wake samples included in this study, nine were narrow-V wakes (0.8% of all wakes), 208 were Kelvin wakes (19.1% of all wakes), 861 were turbulent wakes (78.9% of all wakes), and 13 were internal wave wakes (1.2% of all wakes). In these randomly sampled ship wake SAR images, it was found that turbulent wakes and Kelvin wakes accounted for the majority of the observed ship wakes, with turbulent wakes being observed approximately four times as often as Kelvin wakes. Narrow-V wakes and internal wave wakes were observed far less frequently.

Representative SAR images of the four aforementioned types of ship wakes in the Yellow Sea are shown in Fig. 1. Narrow-V wakes are composed of two bright lines that form a small "V" shape, with half angles between 2°–3°, as shown in Fig. 1(a). Kelvin wakes typically consist of bow waves, stern waves, turbulent waves, cusp waves, transverse waves, and the Kelvin envelope (Oumansour et al., 1994; Sun et al., 2018). In SAR images, bow waves and stern waves are very rarely observed, while cusp waves and transverse waves are only seen in some images. A typical Kelvin wake in a SAR image is generally composed of transverse waves, divergent waves, and the Kelvin envelope, which is defined by two bright lines with an opening of 39°, as shown in Fig. 1(b).

Turbulent wakes were the most common type of wake observed in SAR images, and they usually presented as thin lines behind the courses of ships (Wang and Chen, 2009; Ai et al., 2010; Xu et al., 2018). Along its course, a ship could be located at the center or right side of its wake due to the Doppler Effect, as shown in Fig. 1(c). Based on the bright and dark features of SAR images, turbulent wakes may be categorized as dark or bright turbulent wakes, turbulent wakes with one bright wake and one dark wake, turbulent wakes with two bright wakes and one dark wake, and oil-stained turbulent wakes. Internal wave wakes most commonly appear as multiple "V"-shaped structures in SAR images, as shown in Fig. 1(d). These two types of ship wakes are relatively rare in SAR images.

In this study, we also measured the length of turbulent wakes, and found that 85% of them were shorter than 5 km. However, some oil-stained turbulent wakes were found to have lengths between 10–20 km or longer. Since relatively few Kelvin wakes, narrow-V wakes, and internal wave wakes were detected in this study, their lengths were not analyzed statistically. In our future work, we will collect SAR images for different types of ship wakes and perform more detailed statistical analyses of their lengths.

3 Extraction of ship motion parameters

Ship wake features are closely related to the motion parameters of ships. It is therefore possible to obtain ship motion parameters from different types of wakes via an algorithmic approach by analyzing the wake angles, wake length, and azimuth offset of a ship based on the SAR imaging mechanisms and SAR features of ship wakes. Figure 2 illustrates the ENVISAT ASAR image (100 km × 100 km) of an area in the Yellow Sea near Qingdao that were produced on April 21, 2006 with a pixel size of ~12.5 m, and one ERS-2 SAR image was also imaged of the same area on the same day. In particular, the ENVISAT ASAR image was imaged 29 minutes earlier than the ERS-2 SAR image. Based on SAR images, ship motion parameters were extracted from different types of ship wakes, and the extracted parameters were validated via comparisons with ship parameters that were synchronously co-located by the AIS system.

3.1 Extraction of ship motion parameters from narrow-V wakes

Narrow-V wakes contain short (centimeter-scale) waves and are a manifestation of the surface Bragg wave effect. The theoretical equation derived by Lyden et al. (1988) for the calculation of ship speed based on SAR imaging

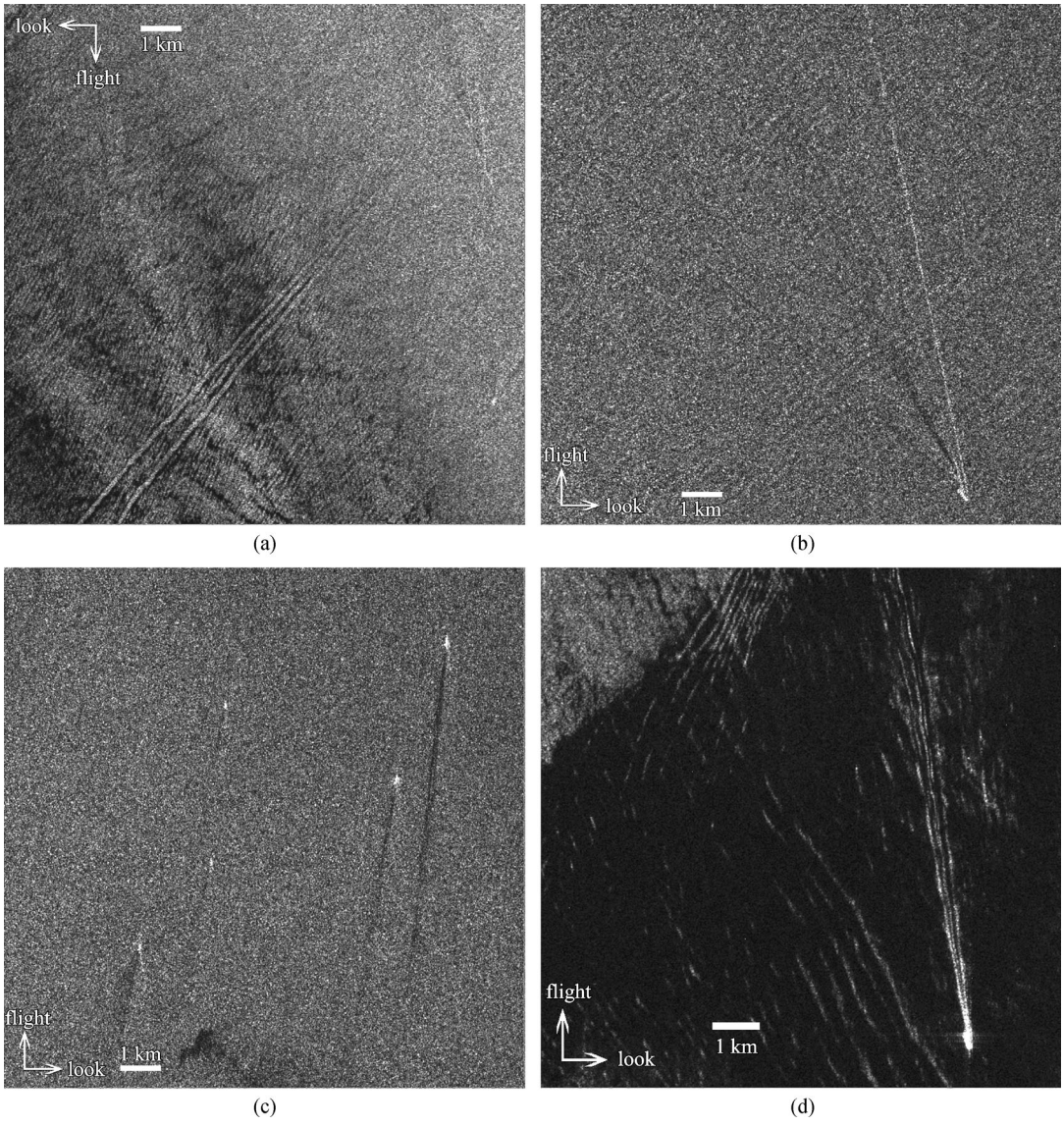

Fig. 1 Representative environmental satellite (ENVISAT) advanced synthetic aperture radar (ASAR) images of ship wakes in the Yellow Sea; pixel size is 12.5 m. (a) Narrow-V wake imaged at 10:06 on April 21, 2006; (b) Kelvin wake imaged at 21:40 on August 17, 2007; (c) turbulent wake imaged at 21:37 on July 29, 2007; (d) internal wave wake imaged at 21:43, July 27, 2005.

mechanisms is (Skoelv et al., 1988):

$$V_{\text{ship}} = \frac{\sin\varphi}{2\tan\alpha}\sqrt{\frac{\lambda g}{4\pi\sin\theta}}. \quad (1)$$

In this equation, φ is the angle between the wake and the side-looking direction, α is the half angle of the narrow-V wake, θ is the radar incidence angle, λ is the wavelength of the radar (Bragg waves), and g is the acceleration of gravity. The length of the narrow-V wave wakes is more than 20 km in Fig. 1(a), which allows the following parameters to be calculated accurately: $\alpha = 2°$, $\phi = 49°$, and $\theta = 25°$; C-band imaging was used to obtain this SAR image. Based on Eq. (1), the speed of this ship was approximately 3.5 m/s. However, since the imaging of narrow-V wakes in SAR images is extremely challenging, narrow-V wakes are not generally reliable for extracting ship motion parameters.

3.2 Extraction of ship motion parameters from Kelvin wakes

Kelvin wakes are composed of features such as transverse waves, divergent waves, and Kelvin arms (Arnold-Bos et al., 2007; Biondi, 2018). According to hydrodynamic theory, the wavelengths of transverse waves are dependent upon ship motion. The theoretical equation given by Lyden et al. (1988) that relates the wavelength of transverse waves in Kelvin wakes to ship speed is (Panico et al., 2017):

$$V_{\text{ship}} = \sqrt{Lg/2\pi}. \quad (2)$$

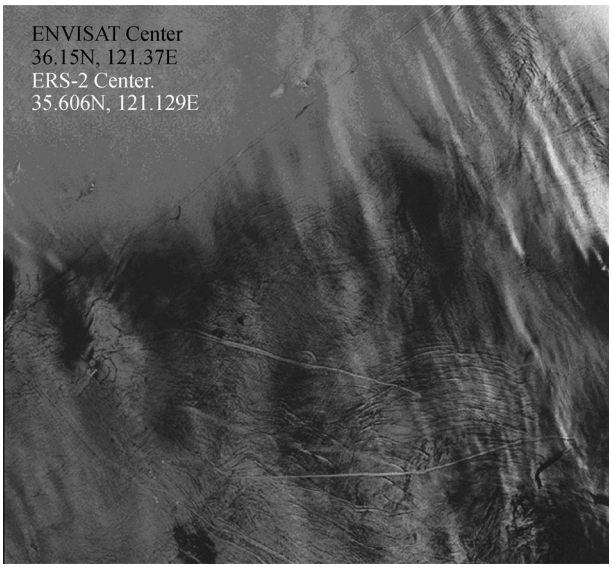

Fig. 2 An ENVISAT ASAR IMP image (100 km × 100 km) of the Yellow Sea near Qingdao acquired at 10:06 on April 21, 2006, and one ERS-2 SAR image was also imaged of the same area 29 minutes later than ENVISAT ASAR.

In this equation, L is the wavelength of the transverse wave component of Kelvin wakes, while g is the gravitational constant.

In the ENVISAT ASAR and ERS-2 SAR images, the wavelengths of the transverse wave component of the Kelvin wake generated by one particular ship were 93.0 m and 99.2 m, respectively. According to Eq. (2), the speeds of this ship were 12.0 m/s and 12.4 m/s in these SAR images. By co-locating with the AIS system, it was found that this ship is the "Ever Diadem", and its speeds at those times were 11.9 m/s and 12.2 m/s, yielding relative errors between the different times of less than 2%.

In reality, it is also possible to obtain ship speed via the spatiotemporal matching of a ship in two sequential SAR images. It was found that the displacement of the ship (i.e., the "Ever Diadem") over 29 minutes was 20.8 km, which corresponds to a ship speed of 12.4 m/s. The ship speeds that were obtained using three different methods are therefore quite similar, confirming the viability and accuracy of ship speed calculations based on the wavelength of transverse waves in Kelvin wakes. However, since the principles that underlie the extraction of ship speed from Kelvin wakes is closely related to gravity waves, ship speed extraction will have a reduced level of accuracy if the imaging of transverse waves in the Kelvin wake is not very clear.

3.3 Extraction of ship motion parameters from turbulent wakes

If the course of a ship contains a component along the range direction of a satellite, an azimuth offset will occur in the SAR image of the ship. In this case, the position of the target ship in the SAR image will deviate by some extent from its actual position, and this characteristically manifests as a separation between the ship and its wake (Graziano et al., 2016). Based on the theories underlying SAR imaging, the speed of a ship may be calculated from its azimuth offset.

$$V_{\text{ship}} = \frac{dV_{\text{sat}}}{H\tan\theta\cos\varphi}. \tag{3}$$

In Eq. (3), d is the azimuth offset of the ship, φ is angle between the motion vector of the ship and the SAR range direction, H is the flight altitude of the SAR platform (satellite), θ is the incidence angle of the radar, and V_{sat} is the flight velocity of the satellite.

Figures 3(a) and 3(b) are sequential ENVISAT and ERS-2 SAR images (10 km × 10 km) of a turbulent wake formed by the same ship imaged on April 21, 2006. The red and green circles in these figures are ship targets, and the green lines represent the turbulent wakes of the labeled ships. The satellite parameters of ENVISAT and ERS-2 were obtained by querying their ephemeris data, while azimuth offsets were calculated from the SAR images. These parameters were then substituted into Eq. (1). It was found that the speed of the ship was 5.5 m/s and 6.8 m/s in the ENVISAT and ERS-2 SAR images, respectively. By co-locating with the AIS system, it was found that the ship in Figs. 3(a) and 3(b) was the "New Vitality," whose recorded speeds were 7.3 m/s and 7.2 m/s at the times corresponding to the SAR images. By comparing the extracted results and field tracking data, it is clear that ship speed can be calculated to a high level of accuracy from the Doppler shifts of a ship, with a relative error of less than 6.5%. However, when the Doppler shift of a moving ship is used to extract its speed and heading, the extraction of ship speed is either impossible or almost certain to result in large errors if the heading of the ship is parallel or near-parallel to the azimuth.

3.4 Extraction of ship motion parameters from internal wave wakes

According to the Keller-Munk model for internal wave wakes, a point source is related to the internal waves it generates by the following geometric relationship, if the point source is moving with a speed of V:

$$\begin{aligned} x &= \frac{\phi V(1-c_p c_g/V^2)}{k(c_p-c_g)}, \\ y &= \frac{\phi c_g(1-c_p^2/V^2)^{\frac{1}{2}}}{k(c_p-c_g)}. \end{aligned} \tag{4}$$

In these equations, ϕ is the phase of the internal wave, k is the wavenumber of the internal wave, (x, y) is the relative

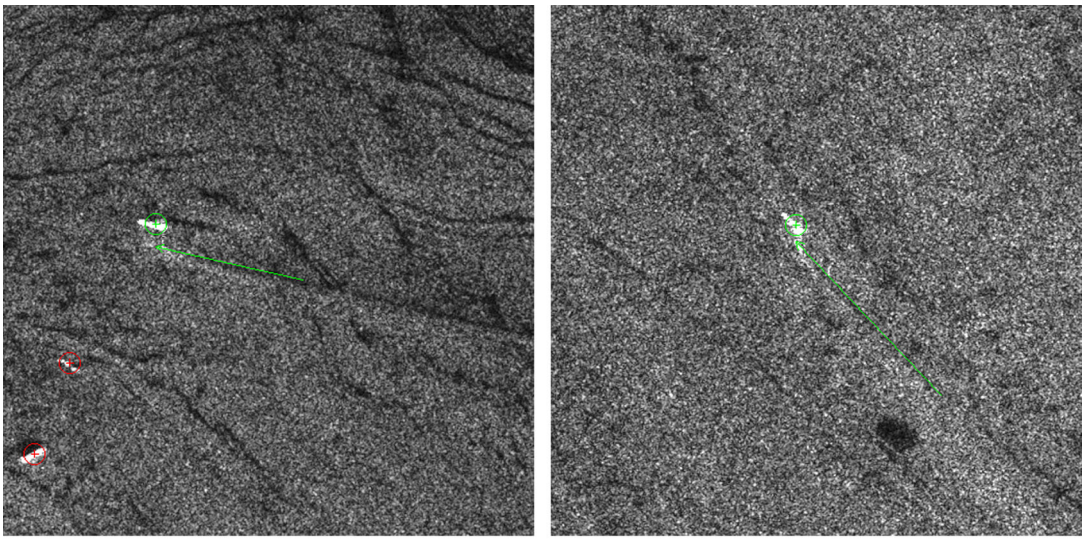

(a) (b)

Fig. 3 Turbulent wake induced by a ship in sequential SAR images (10 km × 10 km). (a) The ENVISAT SAR image at 10:06 on April 21, 2006 and (b) the European Remote-Sensing Satellite 2 (ERS-2) SAR image at 10:35 on April 21, 2006.

displacement of the internal waves from the ship, while group and phase speed, c_g and c_p, are both functions of k. The geometric shape of any wake may be determined by ship speed, V, and the propagation properties of internal waves (c_g and c_p) alone by setting ϕ as a constant, with k as the independent parameter. When the ship speed is much greater than c_g and c_p (i.e., $V >> c_p, c_g$), Eq. (4) may be simplified as:

$$\frac{y}{x} = \frac{c_g}{V} = \tan\alpha, \tag{5}$$

where α is the half angle of the wake.

Figure 4(a) illustrates one internal wave wake in a ENVISAT ASAR sub-image (5 km × 5 km) in the Yellow Sea near Qingdao, which was produced on April 28, 2006 and has a pixel size of ~12.5 m, and the white rectangle in Fig. 4(a) shows the typical spatial features of the internal wave wake. This internal wave wake extends across the diagonal of the image, and the half angle of the opening of the internal wave is α = 1°. Figure 4(b) shows the temperature (T), salinity (S), and density (D) profiles from CTD data that were obtained by the "Dongfanghong No. 2" research vessel from a site in the Yellow Sea near Qingdao on the same day (i.e., April 28, 2006). In the map inset of Fig. 4(b), the black dot is the site where the temperature and salinity profiles was obtained, while the rectangle in Fig. 4(b) is the location of the ENVISAT ASAR imaged.

The water depth of the CTD observation point was 38.6 m, and the corresponding wind speed was 8.1 m/s, with a wind direction of 169°. The depth of the pycnocline was 14 m. Based on the theory underlying waves at fluid interfaces, the group velocity of the internal waves in this cline was c_g = 0.1 m/s. According to Eq. (5), this yields a ship speed of 5.7 m/s. Additionally, the ship speed calculated from the spatiotemporal matching of this ship in the pair of sequential SAR images based on both the ship displacement and the time interval between the sequential SAR images was approximately 5.3 m/s. It is also possible to obtain ship speed via the spatiotemporal matching of a ship in two sequential SAR images. It was found that the displacement of the ship (i.e., the "Ever Diadem") over 29 minutes was 8.9 km, and the speed was 5.1 m/s, which is in close agreement with the ship speed extracted from the internal wave wake. This result further supports the viability and accuracy of the ship speed calculations using internal wave wakes. However, since the generation of internal wave wakes is strongly dependent on the local stratification of seawater, internal wave wakes are difficult to generate under normal circumstances. Therefore, it is not generally possible to use internal wave wakes for the extraction of ship motion parameters.

4 Conclusions

Based on the SAR imaging mechanisms of each type of ship wake, statistical analyses were performed on the features of narrow-V wakes, Kelvin wakes, turbulent wakes, and internal wave wakes using over 1091 ship wake sub-SAR images in the Yellow Sea off of China. The results indicated that turbulent wakes and Kelvin wakes account for the vast majority of ship wakes observed in SAR images, with turbulent wakes occurring four times as frequently as Kelvin wakes. Narrow-V wakes and internal wave wakes are much less common due to the require-

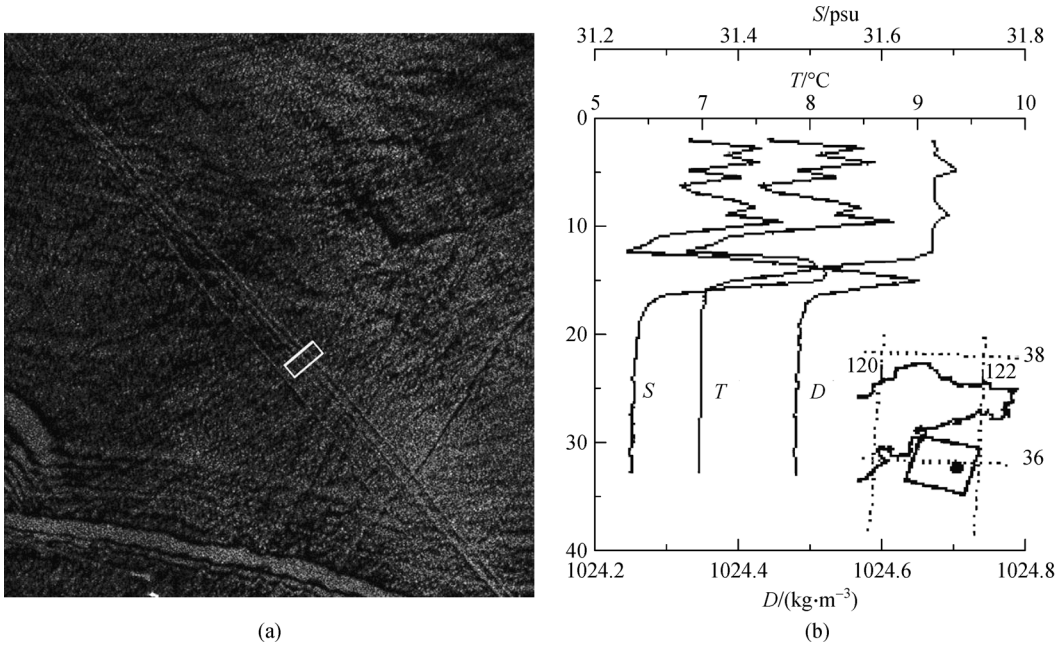

Fig. 4 (a) Internal wave wakes imaged by ENVISAR ASAR in the Yellow Sea on April 28, 2006 and (b) the corresponding temperature (*T*), salinity (*S*), and density (*D*) profiles from temperature, conductivity, and depth (CTD) data.

ments for observing them in terms of both radar system parameters and the marine environment.

The algorithms used for extracting ship motion parameters from each type of ship wake were also analyzed in a targeted manner in this study, based on a deep understanding of the SAR imaging mechanisms and identifying SAR features of each type of ship wake. Additionally, two sequential SAR images of the same area, which were separated by 29 minutes, were also used to extract ship motion parameters. In particular, synchronously measured temperature and salinity profiles from CTD data were used to enable the extraction of ship speeds using internal wave wakes. Based on the results of validation, it was found that the extraction of ship motion parameters from ship wakes is both viable and accurate.

Since SAR images of ship wakes are co-affected by the intrinsic properties of wake-generating ships, the parameters of the SAR system, and marine environmental factors, the identifying SAR features of ship wakes that were obtained in this study and the ship motion parameters extracted from them deviated from reality to some extent. Hence, field data is an absolute necessity for studies on the identifying SAR features of ship wakes. In our future work, we will generate a substantially more extensive dataset using synchronous AIS data, SAR system parameters, synchronous marine environmental data, and marine survey data. This dataset will then be used to study the SAR imaging mechanisms of different types of ship wakes and the quantitative relationships between ship type and marine environmental factors in the identifying SAR features of each type of ship wake. The findings of the present study provide a solid foundation for such further investigations and for the commercialization of SAR-based technologies for detecting ships and extracting ship motion parameters.

Acknowledgements This work is jointly funded by the Shandong Natural Science Foundation (Grant No. ZR2017LD014), the National Natural Science Foundation of China (Grant Nos. 41476088, 41876208, and 41576174), the National Key Projects for Marine Environmental Security (Grant No. 2016YFC1403201) and the National High Resolution Project of China (Grant No. 41Y30B12-9001-14/16). We also appreciate Mrs. Aiqin SHI from State Key Laboratory of Satellite Ocean Environment Dynamics (SOED) of Second Institute of Oceanography for her kindly processing the remote sensing images.

References

Ai J Q, Qi X Y, Yu W, Liu F (2010). A new ship wake CFAR detection algorithm in SAR images based on image segmentation and normalized Hough transform. Journal of Electronic & Information Technology, 32(11): 2668–2673

An Q, Pan Z, You H (2018). Ship detection in Gaofen-3 SAR images based on sea clutter distribution analysis and deep convolutional neural network. Sensors (Basel), 18(2): 334

Arnold-Bos A, Martin A, Khenchaf A (2007). Obtaining a ship's speed and direction from its Kelvin wake spectrum using stochastic matched filtering. Proc Int Geosci Remote Sens Symp, 1106–1109

Biondi F (2018). Low-rank plus sparse decomposition and localized radon transform for ship-wake detection in synthetic aperture radar images. IEEE Geosci Remote Sens Lett, doi: 10.1109/LGRS.2018.2868365

Fan K G, Fu B, Gu Y, Yu X, Liu T, Shi A, Xu K, Gan X (2015). Internal wave parameters retrieval from space-borne SAR image. Front Earth Sci, 9(4): 700–708

Graziano M D, D'Errico M, Rufino G (2016). Ship heading and velocity analysis by wake detection in SAR images. Acta Astronaut, 128: 72–82

Hennings I, Romeiser R, Alpers W, Viola A (1999). Radar imaging of Kelvin arms of ship wakes. Int J Remote Sens, 20(13): 2519–2543

Hogan G G, Chapman R D, Watson G, Thompson D R (1994). Observations of ship-generated internal waves in SAR images from Loch Linnhe, Scotland, and comparison with theory and *in situ* internal wave measurements. IEEE Trans Geosci Remote Sens, 34 (2): 1363–1369

Jackson C R, Apel J R (2004). Synthetic Aperture Radar Marine User's Manual. National Oceanic and Atmospheric Administration

Lyden J D, Hammond R R, Lyzenga D R, Shuchman R A (1988). Synthetic aperture radar imaging of surface ship wakes. Journal of Geophysical Research, 1988, 193: 12293–12300

Melsheimer C, Lim H, Shen C M (1999). Observation and analysis of ship wakes in ERS-SAR and SPOT image. Proceedings of the 20th Asian Conference on Remote Sensing, 22–25

Munk W H (1987). Ship from space. Proceedings of the Royal Society London, A (412): 231–254

Ouchi K (2013). Recent trend and advance of synthetic aperture radar with selected topics. Remote Sensing, 5: 716–807

Ouchi K, Stapleton N R, Barber B C (1997). Multi-frequency SAR images of ship-generated internal waves. Int J Remote Sens, 18(18): 3709–3718

Oumansour K, Wang Y, Saillard J (1994). Application of polarimetric synthetic aperture radar to a ship wake in simulation. Symposium on Antenna Technology and Applied Electromagnetics, Ottawa, Canada, 661–664

Panico A, Graziano M D, Renga A (2017). SAR-based vessel velocity estimation from partially imaged Kelvin pattern. IEEE Geosci Remote Sens Lett, 14(11): 2067–2071

Skoelv A, Wahl T, Eriksen S (1988). Simulation of SAR imaging of ship wakes. Proceedings of IGARSS'88 Symposium, 13–16

Stapleton N R (1997). Ship wakes in radar imagery. Int J Remote Sens, 18(6): 1381–1386

Sun Y, Liu P, Jin Y Q (2018). Ship wake components: isolation, reconstruction, and characteristics analysis in spectral, spatial, and TerraSAR-X image domains. IEEE Trans Geosci Remote Sens, 56 (7): 4209–4224

Swanson C V (1984). Radar Observability of Ship Wakes. Report of Cortana Corporation

Tings B, Velotto D (2018). Comparison of ship wake detectability on C-band and X-band SAR. Int J Remote Sens, 39(13): 4451–4468

Vesecky J F, Stewart R H (1982). The observation of ocean surface phenomena using imagery from the Seasat synthetic aperture radar: an assessment. J Geophys Res, 87(C5): 3397–3430

Wang L L, Chen H X (2009). Multi-ship wakes detection method based on recursive modified Hough transform field. J Syst Eng Electron, 31 (4): 834–837

Xu Z, Tang B, Cheng S (2018). Faint ship wake detection in PolSAR images. IEEE Geoscience & Remote Sensing Letters, 2018, 15(7): 1055–1059

Zilman G, Miloh T (1997). Radar backscatter of a V-like ship wake from a sea surface covered by surfactants. Twenty-first Symposium on Naval hydrodynamics

Zilman G, Zapolski A, Marom M (2004). The speed and beam of a ship from its wake's SAR images. IEEE Trans Geosci Remote Sens, 42 (10): 2335–2343

Zilman G, Zapolski A, Marom M (2015). On detectability of a ship's Kelvin wake in simulated SAR images of rough sea surface. IEEE Trans Geosci Remote Sens, 53(2): 609–619